Nuclear Instruments and Methods in Physics Research B 283 (2012) 59–62

Contents lists available at SciVerse ScienceDirect

Nuclear Instruments and Methods in Physics Research B

journal homepage: www.elsevier.com/locate/nimb

Mean velocity of $5d^56p$ excited tungsten atoms sputtered by Kr^+ ion bombardment

Kenji Motohashi [a,*], Keisuke Nogami [b], Yasuhiro Sakai [b], Hiroyuki A. Sakaue [c], Daiji Kato [c], Takahiro Kenmotsu [d]

[a] Department of Biomedical Engineering, Faculty of Science and Engineering, Toyo University, 2100 Kujirai, Kawagoe-shi, Saitama 350-8585, Japan
[b] Department of Physics, Faculty of Science, Toho University, 2-2-1 Miyama, Funabashi-shi, Chiba 274-8510, Japan
[c] National Institute for Fusion Science, 322-6 Oroshi-cho, Toki-shi, Gifu 509-5292, Japan
[d] Department of Biomedical Engineering, Faculty of Life and Medical Sciences, Doshisha University, Tatara-Miyakodani, Kyotanabe-shi, Kyoto 610-0394, Japan

ARTICLE INFO

Article history:
Received 26 January 2012
Received in revised form 10 April 2012
Available online 28 April 2012

Keywords:
Tungsten surface
Sputtering
Ion-beam induced light emission
Mean velocity

ABSTRACT

Visible emission spectroscopy was conducted for atoms sputtered from tungsten surfaces under Kr^+ ion irradiation (33–60 keV). A number of WI lines were observed in the wavelength of 360–490 nm. The emission intensity of the WI line at 400.88 nm was measured as a function of the distance from the surface. The mean normal velocity of $W^*(5d^5(^6S)6p\ ^7P_4)$ atoms was measured by analyzing the exponential decay curves. No remarkable change in the velocity was found for different projectile energies. The average velocity was $5.6 \pm 1.7\ \mathrm{kms}^{-1}$.

1. Introduction

Tungsten is considered to be the most suitable candidate as plasma-facing materials for International Thermonuclear Experimental Reactor (ITER) because it has many favorable properties [1,2] such as high melting point, high thermal conductivity, low sputtering yield, low tritium retention, and no chemical erosion. However, radiation cooling by tungsten ions in the plasma core is an issue. Tungsten atoms originally sputtered on the wall surface penetrate into the plasma core across the magnetic fields [3]. The penetration depth into the plasma depends on the velocity of the eroded atoms. Thus, it is important to determine the velocity of neutral atoms produced during sputtering of tungsten surfaces. Therefore, in this study, we measured the mean velocity of excited tungsten atoms in the direction normal to the surface by observing ion-beam induced light emission (IBLE).

Although optical emission spectroscopy is one of the most powerful techniques for studying high-temperature plasmas because it does not disturb the plasma, such studies have been scarce. Goehlich et al. measured the angle-resolved velocity distributions of sputtered tungsten atoms by using Doppler-shifted laser-induced fluorescence spectroscopy (DSLF) [4]. Their experimental result for the normal incidence of Ar^+ ions (5 keV) was in good agreement with the Thompson distribution [5] with a high energy falloff corresponding to $n = 2$ in the following equation:

$$f(E) \propto \frac{E}{(E + E_b)^{n+1}}, \tag{1}$$

where E is the kinetic energy of the sputtered atoms, and E_b is the potential energy of the planar surface barrier between the atoms and the solid surface. When their result of $E_b = 8.7$ eV is substituted into the Eq. (1), the mean velocity $\langle v \rangle$ of sputtered tungsten atoms in the ground state is estimated to be $3.7\ \mathrm{kms}^{-1}$.

In contrast, the velocity measurement of excited atoms by observing IBLE is influenced by the survival probability [6,7] of the excited state as we will mention the detail later. In addition, for some metals and semiconductors, this survival probability changes with the surface conditions, especially the amount of oxygen adsorption [6]. In the present study, we measured the mean normal velocity $\langle v_z \rangle$ of excited tungsten atoms sputtered from polycrystalline tungsten surfaces with small oxygen coverage (<0.04) by irradiation with a high flux density ion beam.

2. Experimental apparatus and procedures

The experiment was conducted at a beam line connected with a medium-current ion implanter (ULVAC IM-200MH-FB) at the National Institute for Fusion Science (NIFS). A schematic illustration of the experimental apparatus around the target sample is shown in Fig. 1. A Kr^+ ion beam extracted from a Freeman ion source was introduced into the collision chamber after analyzing the mass to charge ratio (m/e) by using a sector magnet. A polycrystalline tungsten surface (T) set on a movable stage was installed in the collision chamber. An electrode (R) with a 5-mm-diameter hole,

* Corresponding author. Tel.: +81 49 239 1489; fax: +81 49 231 5026.
E-mail address: motohashi@toyo.jp (K. Motohashi).

0168-583X/$ - see front matter © 2012 Elsevier B.V. All rights reserved.
http://dx.doi.org/10.1016/j.nimb.2012.04.016

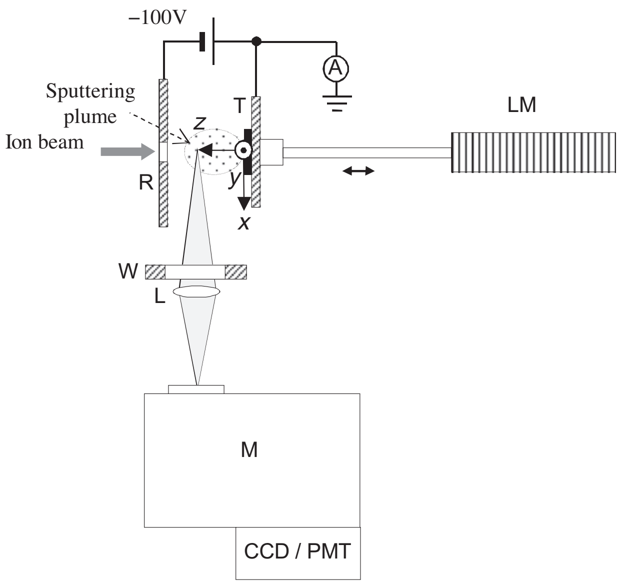

Fig. 1. Schematic illustration of the experimental apparatus around the target sample.

which applied −100 V to the surface, was also installed at 30 mm in front of the target to retard secondary electrons. The ion beam was perpendicular to the tungsten surface. The stage could be moved in a direction parallel to the ion beam axis within a range of 50 mm by using a linear motion feedthrough (LM).

After passing through a quartz window (W) and a condenser lens (L), the light from the sputtered atoms was focused onto the entrance slit of a monochromator (M) equipped with a charge coupled device (CCD) or a photo-multiplier tube (PMT). The optical axis crossed the ion beam axis at a right angle because it was positioned parallel to the surface. We measured the light intensity as a function of the distance z from the surface by moving the stage linearly, where $z = 0$ was defined as the position where the intensity is maximum [8].

The pressure of the chamber was maintained below 7×10^{-5} Pa by a turbo molecular pump during the measurements. It reached less than 1×10^{-5} Pa when the ion beam did not irradiate the tungsten surface. The current of the Kr^+ ion beam was about 30 μA. A relatively high current density (=150 μA/cm^2) maintained the oxygen coverage on the surface at equilibrium $\Theta \ll 1$, which was estimated by the following approximation [9]:

$$\Theta \approx \frac{C_S \Phi_O}{C_S \Phi_O + S_O \Phi_i} \tag{2}$$

where Φ_O is the particle flux density of incoming oxygen molecules, Φ_i is the particle flux density of incident Kr^+ ions, and C_S and S_O are the initial sticking and sputtering coefficients for oxygen atoms on a tungsten surface, respectively. Θ is estimated to be less than 0.04 by assuming $\Phi_i \sim 1 \times 10^{15}$ cm^{-2}s^{-1}, $\Phi_O \sim 1 \times 10^{14}$ cm^{-2}s^{-1}, $C_S < 0.4$, and $S_O > 1$ [10–15] for the experimental conditions of room temperature along with the oxygen partial pressure evaluated from the chamber pressure and ion beam current density mentioned above.

3. Results and discussion

Fig. 2 shows a typical survey spectrum in the wavelength of 360–490 nm under Kr^+ (33 keV) irradiation. This spectrum was measured with the PMT detector in the single photon counting mode, and no correction to the optical efficiency and no subtraction of background photons were performed. A number of lines from

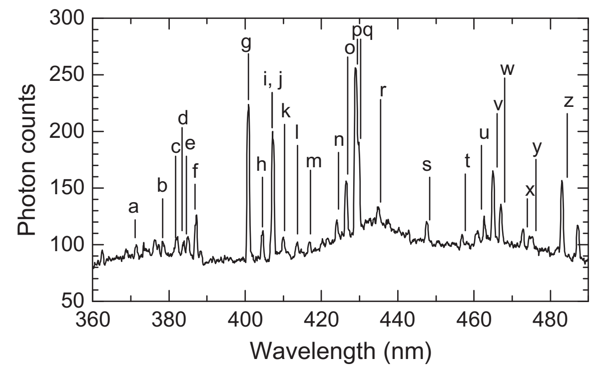

Fig. 2. Survey optical emission spectrum obtained by the PMT detector under Kr^+ (33 keV) irradiation of a polycrystalline tungsten surface. Labels a–z denote strong lines observed in the spectrum; properties of these lines are given in Table 1.

Table 1
Strong lines of the visible emission spectrum observed for tungsten surfaces under irradiation by Kr^+ (33 keV) ions.

Labels	Wavelength (nm) [16]	Species	Transitions [16]
a	371.80, 371.86, 372.14	KrII	$4s^24p^4(^1D)5d\ ^2G_{9/2} \rightarrow 4s^24p^4(^1D)5p\ ^2F_{7/2}$
b	377.80, 378.31	KrII	$4s^24p^4(^3P)5d\ ^4F_{9/2,\ 7/2} \rightarrow 4s^24p^4(^3P)5p\ ^4D_{7/2,\ 5/2}$ $4s^24p^4(^3P)5d\ ^2F_{7/2} \rightarrow 4s^24p^4(^3P)5p\ ^2D_{5/2}$
c	381.75	WI	$5d^46s(^6D)6p\ ^5F_3 \rightarrow 5d^5(^6S)6s\ ^7S_3$
d	383.51	WI	$5d^46s(^6D)6p\ ^5P_2 \rightarrow 5d^46s^2\ ^5D_2$
e	384.62, 384.75	WI	$5d^46s(^6D)6p\ ^5F_{2,\ 1} \rightarrow 5d^46s^2\ ^5D_{1,\ 0}$
f	386.80	WI	$5d^46s(^6D)6p\ ^7D_4 \rightarrow 5d^5(^6S)6s\ ^7S_3$
g	400.88	WI	$5d^5(^6S)6p\ ^7P_4 \rightarrow 5d^5(^6S)6s\ ^7S_3$
h	404.56	WI	$5d^46s(^6D)6p\ ^5F_2 \rightarrow 5d^5(^6S)6s\ ^7S_3$
i	407.00	WI	$5d^46s(^6D)6p\ ^5P_2 \rightarrow 5d^46s^2\ ^5D_3$
j	407.44	WI	$5d^5(^6S)6p\ ^7P_3 \rightarrow 5d^5(^6S)6s\ ^7S_3$
k	410.27	WI	$5d^46s(^6D)6p\ ^5P_3 \rightarrow 5d^46s^2\ ^5D_4$
l	413.75	WI	$5d^5(^6S)6p\ ^7P_3 \rightarrow 5d^46s^2\ ^5D_2$
m	417.12	WI	$5d^46s(^6D)6p\ ^7D_4 \rightarrow 5d^46s^2\ ^5D_3$
n	424.44	WI	$5d^46s(^6D)6p\ ^7D_5 \rightarrow 5d^46s^2\ ^5D_4$
o	426.94	WI	$5d^5(^6S)6p\ ^7P_2^{\dagger} \rightarrow 5d^5(^6S)6s\ ^7S_3$
p	429.46	WI	$5d^5(^6S)6p\ ^7P_2^{\ddagger} \rightarrow 5d^5(^6S)6s\ ^7S_3$
q	430.21	WI	$5d^46s(^6D)6p\ ^7D_3 \rightarrow 5d^5(^6S)6s\ ^7S_3$
r	435.55	KrII	$4s^24p^4(^3P)5p\ ^4D_{7/2} \rightarrow 4s^24p^4(^3P)5s\ ^4P_{5/2}$
s	448.42	WI	$5d^46s(^6D)6p\ ^7D_2 \rightarrow 5d^46s^2\ ^5D_1$
t	457.72	KrII	$4s^24p^4(^1D)5p\ ^2F_{7/2} \rightarrow 4s^24p^4(^1D)5s\ ^2D_{5/2}$
u	461.92	KrII	$4s^24p^4(^3P)5p\ ^2D_{5/2} \rightarrow 4s^24p^4(^3P)5s\ ^2P_{3/2}$
v	465.99	WI	$5d^46s(^6D)6p\ ^7D_1 \rightarrow 5d^46s^2\ ^5D_0$
w	468.05	WI	$5d^46s(^6D)6p\ ^7D_3 \rightarrow 5d^46s^2\ ^5D_3$
x	473.90	KrII	$4s^24p^4(^3P)5p\ ^4P_{5/2} \rightarrow 4s^24p^4(^3P)5s\ ^4P_{5/2}$
y	476.24, 476.57	KrII	$4s^24p^4(^3P)5p\ ^2D_{3/2},\ ^4D_{5/2} \rightarrow 4s^24p^4(^3P)5s\ ^2P_{1/2},\ ^4P_{3/2}$
z	484.38	WI	$5d^46s(^6D)6p\ ^7D_2 \rightarrow 5d^46s^2\ ^5D_2$

† Lande $g = 0.87$.
‡ Lande $g = 1.84$.

sputtered tungsten atoms and backscattered Kr ions were observed. The wavelengths and transitions of strong lines (labeled a–z) [16] are summarized in Table 1. Although all WI lines belong to 6p→6s/5d transitions, they are classified into four types of transitions that consist of a combination of two upper and two lower states: $5d^56p \rightarrow 5d^56s$ (g, j, o, and p), $5d^56p \rightarrow 5d^46s^2$ (l), $5d^46s6p \rightarrow 5d^56s$ (c, f, h, and q), and $5d^46s6p \rightarrow 5d^46s^2$ (d, e, i, k, m, n, s, v, w, and z). KrII lines are classified into two types of transitions: 5d → 5p (a and b) and 5p → 5s (r, t, u, x, and y). Fig. 3a shows a high-resolution spectrum obtained by the CCD detector in the